

Development of a low-background neutron detector array

Y. T. Li,^{1,2} W. P. Lin,^{3,*} B. Gao,^{1,2,4,†} H. Chen,¹ H. Huang,⁴ Y. Huang,³ T. Y. Jiao,^{1,2} K. A. Li,^{1,2} X. D. Tang,^{1,2,4} X. Y. Wang,^{1,2} X. Fang,⁵ H. X. Huang,⁶ J. Ren,⁶ L. H. Ru,^{1,2} X. C. Ruan,⁶ N. T. Zhang,^{1,2} and Z. C. Zhang^{1,2}

¹CAS Key Laboratory of High Precision Nuclear Spectroscopy,

Institute of Modern Physics, Chinese Academy of Sciences, Lanzhou 730000, China

²School of Nuclear Science and Technology, University of Chinese Academy of Sciences, Beijing 100049, China

³Key Laboratory of Radiation Physics and Technology of the Ministry of Education, Institute of Nuclear Science and Technology, Sichuan University, Chengdu 610064, China

⁴Joint Department for Nuclear Physics, Lanzhou University and Institute of Modern Physics, Chinese Academy of Sciences, Lanzhou 730000, China

⁵Sino-French Institute of Nuclear Engineering and Technology,

Sun Yat-sen University, Zhuhai, Guangdong 519082, People's Republic of China

⁶China Institute of Atomic Energy, Beijing 102413, People's Republic of China

A low-background neutron detector array was developed to measure the cross section of the $^{13}\text{C}(\alpha, n)^{16}\text{O}$ reaction, which is the neutron source for the s -process in AGB stars, in the Gamow window ($E_{c.m.} = 190 \pm 40$ keV) at the China Jinping Underground Laboratory (CJPL). The detector array consists of 24 ^3He proportional counters embedded in a polyethylene cube. Due to the deep underground location and a borated polyethylene shield around the detector array, a low background of 4.5(2)/hour was achieved. The $^{51}\text{V}(p, n)^{51}\text{Cr}$ reaction was used to determine the neutron detection efficiency of the array for neutrons with energy $E_n < 1$ MeV. Geant4 simulations, which were shown to well reproduce experimental results, were used to extrapolate the detection efficiency to higher energies for neutrons emitted in the $^{13}\text{C}(\alpha, n)^{16}\text{O}$ reaction. The theoretical angular distributions of the $^{13}\text{C}(\alpha, n)^{16}\text{O}$ reaction were shown to be important in estimating the uncertainties of the detection efficiency.

Keywords: Underground laboratory , Neutron detector , Low background , ^3He Counter

I. INTRODUCTION

The $^{13}\text{C}(\alpha, n)^{16}\text{O}$ reaction is the dominant neutron source for the slow neutron capture process (s -process), which synthesized roughly half of the elements heavier than iron in the Universe [1]. The main site of the s -process is the “He inter-shell” of asymptotic giant branch (AGB) stars where the temperature is 0.1 GK. This corresponds to a Gamow window of 190 ± 40 keV for the $^{13}\text{C}(\alpha, n)^{16}\text{O}$ reaction, which is far below the Coulomb barrier. Theoretical calculations predicted the cross section as low as $\sim 10^{-14}$ barn at 190 keV [2, 3]. Meanwhile, the $^{13}\text{C}(\alpha, n)^{16}\text{O}$ reaction is also the main neutron source for the intermediate neutron capture process (i -process) with a typical temperature 0.2 GK [4, 5]. A reliable direct measurement is still missing within the corresponding energy range from 0.2 to 0.54 MeV. To push direct measurements of the cross section towards the Gamow window, high-intensity beams and low-background neutron detector array are indispensable.

Present measurements performed at ground laboratories are limited by the cosmic-ray-induced background. With a typical background counting rate of a few hundred per hour (e.g. [6, 7]), those measurements only reached a lower limit of $E_\alpha \sim 400$ keV with a cross section of $\sim 10^{-10}$ barn. The China JinPing underground Laboratory (CJPL) [8] with about 2400 m rock overburden (6700 m water equivalent) shields against most of the cosmic rays. The ultra-low

background provides new opportunities for neutrino physics [9], search of dark matter [10, 11] and direct cross section measurements of key reactions in nuclear astrophysics [12, 13]. The Jinping Underground Nuclear Astrophysics experimental facility (JUNA) [12, 13] has been initiated to measure important stellar nuclear reaction rates, taking advantage of the low-background environments in CJPL. The present JUNA project includes $^{12}\text{C}(\alpha, \gamma)^{16}\text{O}$, $^{13}\text{C}(\alpha, n)^{16}\text{O}$, $^{19}\text{F}(p, \gamma)^{20}\text{Ne}$ and $^{25}\text{Mg}(p, \gamma)^{26}\text{Al}$ reactions [12, 13]. A high-intensity accelerator capable of delivering proton and α beams up to 10 mA in the energy range of 0.05 - 0.4 MeV has been built for JUNA [12]. This made it possible to measure the $^{13}\text{C}(\alpha, n)^{16}\text{O}$ cross section at the region of the s -process Gamow window if combined with a high-efficiency and low-background neutron detection system.

This paper describes the development and characterization of a low-background neutron detector array for the cross section measurement of the $^{13}\text{C}(\alpha, n)^{16}\text{O}$ reaction.

II. DESIGN OF THE DETECTOR ARRAY

The detector array consists of 24 ^3He -filled proportional counters (manufactured by GE-Reuter Stokes) embedded in a $50 \times 50 \times 50$ cm³ polyethylene cube. Each proportional counter is filled with ^3He and argon gases, with pressures of 4 bar and 2.4 bar, respectively. The active length of each counter is 30 cm with a diameter of 2.54 cm. The sketch of the detector array is shown in Fig. 1. The 24 proportional counters are evenly distributed in two concentric rings with radius of $R_1 = 8.5$ cm and $R_2 = 13$ cm, respectively. The radius of the two rings were optimized using Geant4 simulations,

* Corresponding author, linwp1204@scu.edu.cn

† Corresponding author, gaobsh@impcas.ac.cn

following the same procedure as that in [14], to get the maximum detection efficiency for 2.0-MeV isotropic neutrons. A central bore hole with a diameter of 10 cm was created to accommodate the beam line and the target. Neutrons from the $^{13}\text{C}(\alpha, n)^{16}\text{O}$ reaction with energies of 2 - 3 MeV are first moderated by the polyethylene cube and then captured by the proportional counters. To shield against environmental neutrons, the polyethylene cube is wrapped with a 5 cm-thick 7% borated polyethylene layer.

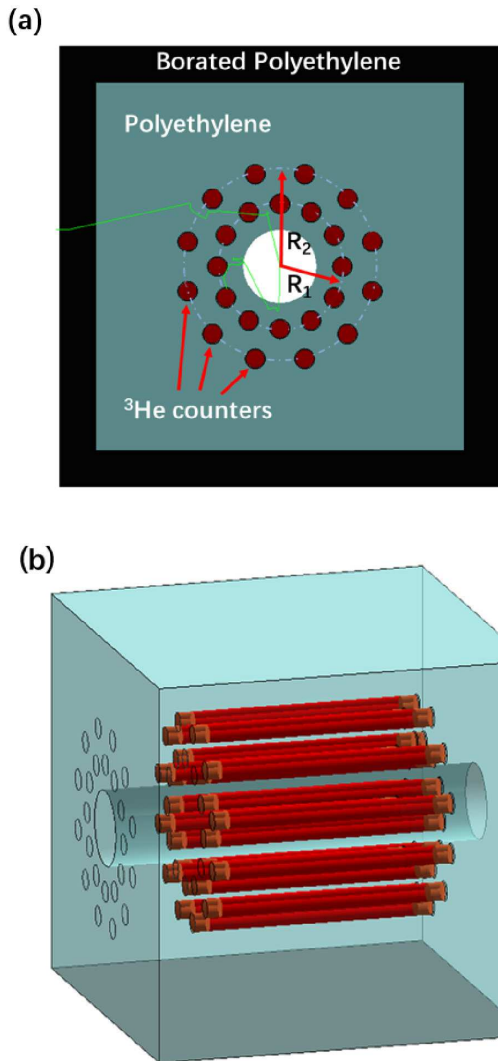


Fig. 1. (Color online) Schematic view of the detector array. In panel (a), the borated polyethylene shield (black brick), positions of the ^3He counters (red tubes) and the central bore hole are indicated. Traces of two neutron events are also shown as green curves. In panel (b), a three-dimensional view of the detector array is presented.

The signal of each detector is processed by a charge-sensitive pre-amplifier (model CAEN A1422). The output waveforms are digitized and recorded by a XIA Pixie-16 100 MHz card. Fig. 2 (a) shows a typical energy spectrum measured by the detector array using a ^{252}Cf source. The “Neutron & alpha” cut as shown in Fig. 2 (b) was used in the plot

to select the neutron events (see the following sections for details). The peak at 0.76 MeV corresponds to full-energy events where the triton and proton produced from the $^3\text{He} + n \rightarrow p + t$ reaction deposit all their kinetic energies in the sensitive region of the counter. If the proton or triton hits the wall of the detector before depositing all their kinetic energies in the sensitive region, the detector records only part of the reaction Q value. Those are wall-effect events which correspond to the flat region with lower energies starting from 0.18 MeV in the spectrum. The argon gas filled in the proportional counters has little effect on the neutron detection efficiency but can significantly decrease the track lengths of the produced proton and triton, and therefore reduce the wall effect. By defining a region of interest around the full energy peak between 0.64 - 0.8 MeV (ROI) as indicated in Fig. 2 (a), we find $81.0 \pm 0.4\%$ of the detected events are located in it.

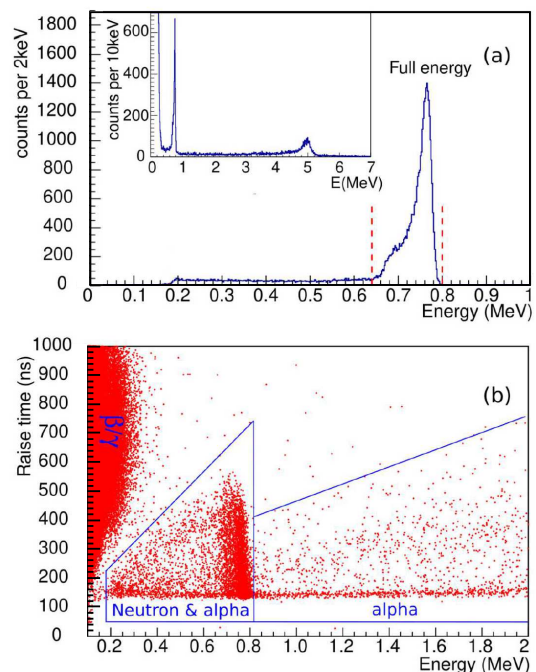


Fig. 2. (Color online) (a) Typical energy spectrum measured by the detector. A cut as shown in panel (b) was applied to select the neutrons (see text). The dashed lines indicate the regions of interest between 0.64 - 0.8 MeV. The inset shows an energy spectrum in wider energy range without cuts. (b) Raise time versus energy two-dimensional plot measured by the detector array. The β/γ -, neutron & alpha- and alpha-regions are indicated in the plot.

III. BACKGROUND MEASUREMENTS

Stainless steel is chosen as the wall material of the proportional counters because it has much lower α emission rate comparing to aluminum [15, 16]. The inset in Fig. 2 (a) shows an energy spectrum up to 7 MeV measured at the CJPL. The events located beyond the neutron full-energy peak are mainly due to α radioactivity from the wall material

of the counters. The α spectrum has a relatively flat distribution below ~ 3 MeV and shows a peak at 5 MeV, a typical energy of α decays from U/Th nuclides. Below 0.3 MeV energy region, lots of γ/β events exist, overlapping with the neutron events. Following the procedure described in Ref. [15], the β/γ events can be well separated from neutrons in the raise time versus energy two-dimensional plot as shown in Fig. 2 (b) taken at the CJPL.

To characterize the background of the detector array, ground- and underground-measurements were performed at the China Institute of Atomic Energy and the A1 hall of the CJPL, respectively. The neutron events were selected by using the "neutron & alpha" cut from the raise time versus energy two-dimensional plot as shown in Fig. 2 (b). Such events also include contributions from α background. To disentangle the α backgrounds from the "neutron & alpha" events, a flat α energy spectrum is assumed [15, 16] in the energy range 0.18 - 2.0 MeV. The total background inside the "neutron & alpha" cut as shown in Fig. 2 (b) measured at CJPL for the whole array is 4.5(2)/hour, of which 1.94(5)/hour is from α background. The above α background is evaluated using the α counts in the energy range 1.0 - 2.0 MeV which was assumed to have the same α emission rate as 0.18 - 0.8 MeV. This assumption was verified using a ^4He proportional counter which will be discussed below. The total background is more than two orders of magnitude lower than the result of 1238(11)/hour obtained from ground-measurement.

A ^4He counter, which has exactly the same parameters as the ^3He counters but filled with ^4He gas instead of ^3He , manufactured by the same supplier was used to investigate the α background in more detail. The ^4He counter is insensitive to neutrons but expected to have similar α background shape as the ^3He counters. The α background rate, with 28.9-hour measurement time in CJPL, was found to be 4.24 ± 0.48 and $4.22 \pm 0.38 \text{ MeV}^{-1}\text{hour}^{-1}$, in 0.18 - 0.8 and 1.0 - 2.0 MeV energy regions, respectively. This justifies that the two energy regions have indeed the same α emission rates. However, we found an α emission rate of 2.63(30)/hour by using the same neutron cut as the ^3He counters in the raise time versus energy plot. This is about a factor of 30 higher than the ^3He counters. Note that the α emission rate of 1.94(5)/hour quoted above includes the background of the 24 ^3He counters while the 2.63(30)/hour is only for one ^4He counter. This implies that the α background could differ significantly even for the same type of wall material. This has to be carefully investigated at the manufacturing stage in order to achieve low α background.

To further reduce the α background, one can choose the events within the ROI only [see Fig. 2 (a)]. As a result, the α background is reduced by 74% at the cost of losing only about 19% of the neutron detection efficiency. This corresponds to a background of 2.5(1)/hour, of which 0.50(1)/hour is from α background. A better approach for α -background suppression is to use plastic scintillator as the moderator, where most of the α background can be eliminated via coincident measurements [17]. The α background is intrinsic properties of the proportional counters used in the array which does not change with environments. However, the neutron background

may change with different environments and therefore should be characterized for each use.

IV. EFFICIENCY CALIBRATION

A. $^{51}\text{V}(p, n)^{51}\text{Cr}$ Experiment and simulation

Detection efficiency of the array was calibrated at the nuclear physics experiment (NPE) terminal of the 3-MV tandemron accelerator [18] at Sichuan university. The detection efficiency hereafter includes both full-energy and wall-effect events. Quasi Mono-energetic neutrons were produced using the $^{51}\text{V}(p, n)^{51}\text{Cr}$ reaction ($Q = -1534.8$ keV) at incident energies between 1.7 and 2.6 MeV with a step of 0.15 MeV. The $^{51}\text{V}(p, n)^{51}\text{Cr}$ reaction is widely used in the calibration of neutron detectors [14, 16, 19–22] for its slow variation of neutron intensity and energy with angle, and the well-known target preparation and utilization. Fig. 3 shows the emitted neutron energy as a function of incident proton beam energy. When the incident energy is above 2.33 MeV, neutrons from transitions feeding the first excited state of ^{51}Cr ($E_x = 749$ keV) are mixed with those feeding the ground state. However, as pointed out in Ref. [16], the contribution from transitions to the first excited state is negligible for incident energies up to 2.6 MeV [19], which was also confirmed in the present work (see discussions in the following sections). The proton beams were focused at the target with a diameter of less than 5 mm (full width at half maximum). The beam spots were monitored by a fluorescent target together with a beam position monitor located 1.5 m upstream the target for each beam energy.

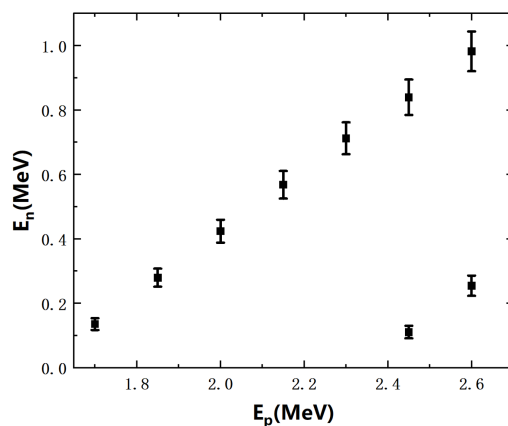


Fig. 3. The emitted neutron energies from the $^{51}\text{V}(p, n)^{51}\text{Cr}$ reaction as a function of proton beam energies. The height of the bars represents the energy spread of the emitted neutrons. The two components of the neutron energies at $E_p = 2.45$ and 2.6 MeV correspond to transitions feeding the ground and the first-excited states of ^{51}Cr .

Vanadium targets with a thickness of $110 \mu\text{g}/\text{cm}^2$ were used in the measurements. They were produced by evaporating natural vanadium on 1-mm thick tantalum disks with a

diameter of 30 mm. The target thickness corresponds to an energy loss of 8~11 keV for proton beams with energies of 1.7 - 2.6 MeV. The beam intensity varied from 4 μA to 120 nA as the beam energy increased from 1.7 to 2.6 MeV, making the counting rate of the detector array stay around $10^4/\text{s}$ with a dead time being less than 1% for all beam energies. A direct water cooling of the reaction target was used to reduce the sputtering and target loss. The possible contribution of beam induced background was investigated with a blank tantalum target at the beam energy of 2.0 MeV. The background contribution was found to be less than 1%.

The total number of emitted neutrons was determined based on the activation method as described in Ref. [16]. The number of radioactive product ^{51}Cr equals to the number of emitted neutrons in the reaction. ^{51}Cr decays by electron capture with a half-life of $T_{1/2} = 27.7025(24)$ days and has a branching ratio of $B = 9.91(1)\%$ to decay to the first excited state of its daughter nuclei ^{51}V , which is followed by the emission of a 320-keV γ ray. The off-line measurement of this γ ray was carried out with a GEM series HPGe detector whose relative efficiency is 30%. The absolute efficiency of the HPGe detector was measured at a distance of 20 cm using ^{137}Cs [$1.534(19)\times 10^5$ Bq] and ^{152}Eu [$5.72(6)\times 10^4$ Bq] γ -ray sources. The distance of 20 cm is large enough to avoid pileups of cascading γ rays from the sources. A ^{51}Cr γ source was produced by the $^{51}\text{V}(p, n)^{51}\text{Cr}$ reaction. Its activity was measured at the position of 20 cm and then used to determine the efficiency for the 320-keV γ line at the position of 10.2 cm (η_{320}), where all the irradiated targets were placed for off-line measurements. η_{320} was determined to be 0.498(7)% at 10.2 cm. As beam current was stable within the irradiation time, the number of emitted neutrons was then determined by the off-line measurement of the 320 keV γ ray with the activation formula [16]

$$N_R = \frac{N_\gamma}{B \cdot \eta_{320}} \cdot \frac{e^{\lambda t_w}}{1 - e^{-\lambda t_c}} \cdot \frac{\lambda \cdot t_i}{1 - e^{-\lambda t_i}}, \quad (1)$$

where N_γ , t_i , t_c and t_w are the number of detected 320-keV γ rays, the activation time, the counting time, and the waiting time elapsed between the end of irradiation and the start of the counting. $\lambda = \ln(2)/T_{1/2}$ is the decay constant of ^{51}Cr . After dead time correction, the detection efficiency of the neutron detector is calculated as

$$\eta_n = \frac{N_n}{N_R}, \quad (2)$$

where N_n is the detected number of neutrons by the detector array.

Since the energy of the neutrons emitted in the $^{51}\text{V}(p, n)^{51}\text{Cr}$ reaction is only up to ~ 1 MeV, it is still far below that from $^{13}\text{C}(\alpha, n)^{16}\text{O}$ reaction. The Monte Carlo simulation code Geant4 [23, 24] of version 10.4.6 was used to determine the neutron detection efficiency at neutron energies above 1 MeV.

The detailed detector setup used the simulation is shown in Fig. 4. The beam pipe, target backing and water cooling loops were included in the simulation, which resembles the

real physical setups. An overestimation of the neutron detection efficiency was obtained from the simulation compared to the experimental results. Similar overestimations have also been observed in several other setups [14, 16]. This overestimation is interpreted as that some of the neutrons are absorbed by small contaminants in the moderating polyethylene. Instead of using a normalization factor, we added a small amount of boron into the moderating polyethylene in the simulation to take into account the neutron absorption effects. Fig. 5 (a) shows the reduced χ^2 , obtained by comparing the simulated and measured detection efficiencies, as a function of boron mass fraction. The minimum of χ^2 was found at the boron mass fraction of 0.054% by fitting the curve using a parabola. The simulated total, inner ring and outer ring detection efficiencies are shown in Fig. 5 (b). An estimation of the first excited state contributions was also carried out using the first excited state neutron component estimated from a statistic model calculation, calibrated using the experimental data [19], using TALYS [25]. The simulated total efficiencies with the first state neutron contributions are also shown as the blue short dashed curve in Fig. 5 (b). The maximum deviation between the simulation with and without the contribution of the first excited state is 0.9%, which is ineligible by comparing to the experimental uncertainty of 3.7%.

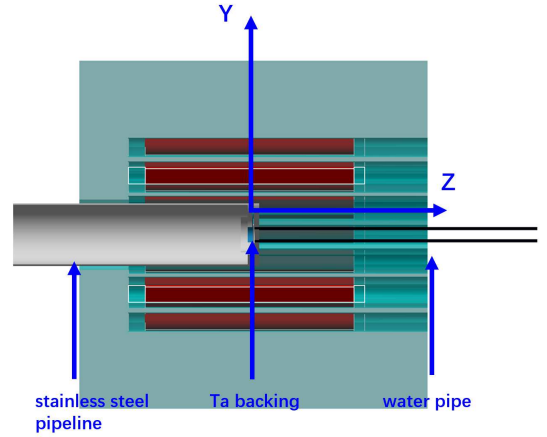


Fig. 4. (Color online) The detector setup used in the simulations for the $^{51}\text{V}(p, n)^{51}\text{Cr}$ reaction.

The boron contaminant affects not only the total efficiency, but also the ratio $R_{in/out}$ of the detection efficiencies of the inner and the outer ring detectors. With the boron mass fraction obtained above, the measured ratio $R_{in/out}$ is also well reproduced by the two simulations (see Fig. 5 (c)). Except for the first point, the simulation results are 1%-3% lower than that of the experiment at $E_p < 2.4$ MeV. Note that the isotropic angular distributions are used in the simulations. The discrepancy of $R_{in/out}$ between simulations and experiment is probably due to the non-isotropic distribution of the emitted neutrons. For $E_p = 2.45$ and 2.6 MeV, the discrepancy between the simulated (with ground state neutrons) and measured $R_{in/out}$ ratios starts to increase to 1.6% and 5%, respectively. This is due to the opening of the decay channel to the first excited state in ^{51}Cr (see Fig. 3). Taking into ac-

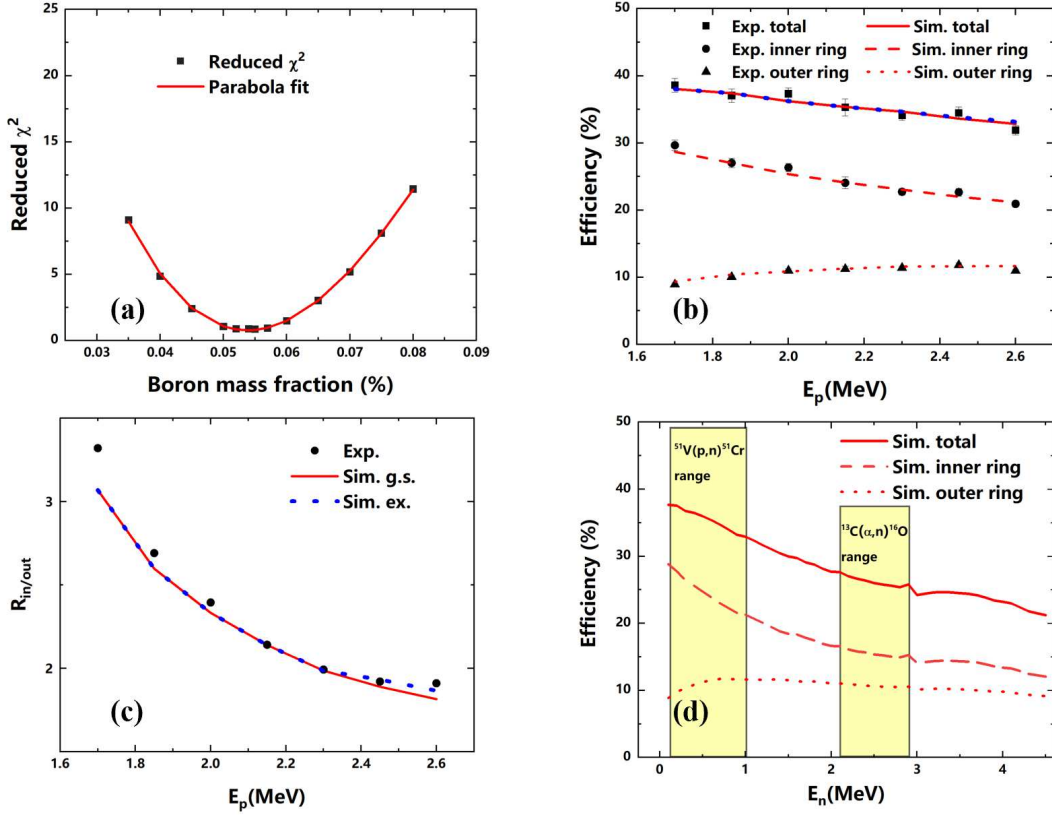


Fig. 5. (Color online) (a) The reduced χ^2 , obtained by comparing the simulated and measured total detection efficiencies, as a function of boron mass fraction. The curve is a parabola fitting of the reduced χ^2 . (b) Measured and simulated total, inner ring and outer ring detection efficiencies as a function of proton beam energy in the $^{51}\text{V}(p,n)^{51}\text{Cr}$ reaction. Blue short dashed curve represents the simulation with first excited state neutrons. The first excited state neutron component were estimated from a statistical model calculation, calibrated using the experimental data [19], using TALYS [25]. (c) Measured and simulated inner-to-outer-ring ratios $R_{in/out}$ at different proton beam energies. (d) Simulated total, inner ring and outer ring detection efficiencies for mono-energetic neutrons with an isotropic angular distribution. The neutron range indicated with $^{13}\text{C}(\alpha,n)^{16}\text{O}$ is for the α energy range $E_\alpha = 300 - 800$ keV.

count the first excited state neutrons estimated from TALYS, the discrepancy is reduced to 0.6% and 2.3% for $E_p = 2.45$ and 2.6 MeV, respectively, as shown in Fig. 5 (c).

The contributions from the decay channel to the first excited state is negligibly small regarding the total detection efficiency though its effects on the $R_{in/out}$ is larger. The total, inner ring and outer ring detection efficiencies for mono-energetic neutrons up to 4.5 MeV with an isotropic angular distribution were also simulated and shown in Fig. 5 (d).

The dependence of detection efficiency on the source position was measured by placing the detector array at different positions along the beam line (Z axis) using the $^{51}\text{V}(p,n)^{51}\text{Cr}$ reaction at $E_p = 2$ MeV. The position $Z = 0$ corresponds to the target being at the center of the array. Moving the detector array forward in the beam direction corresponds to positive Z values and backward corresponds to negative Z values. The relative efficiencies at different positions were normalized using integrated incident beam currents on the target. The results for the total, inner ring and outer ring detectors are shown in Fig. 6 together with the Geant4 simulations. In Fig. 6, the measured total efficiency at $Z = 0$ was normalized to the simulated value. Overall good agreements were

found between the measurements and the simulations.

Taking into account the average deviation between the experimental data and simulations between Fig. 5 (b) and Fig. 6, the difference between the Geant4 simulations and the experiment results is 2.8%, which reflects one of the systematic uncertainties of our simulation and is quoted as the uncertainty of the Geant4 simulations.

B. Extrapolating the detection efficiency for the study of the $^{13}\text{C}(\alpha,n)^{16}\text{O}$ reaction at stellar energies

It should be noted that the simulated efficiency in Fig. 5 cannot be directly applied to the $^{13}\text{C}(\alpha,n)^{16}\text{O}$ reaction in which the emitted neutrons are neither mono-energetic nor isotropic. The asymmetry in the efficiency curve shown in Fig. 6 indicates that the simulation predicts a slightly higher detection efficiency for neutrons emitted at backward angles than that at forward angles. Since the angular distribution of the $^{13}\text{C}(\alpha,n)^{16}\text{O}$ reaction is not measured at low energies close to the Gamow window, theoretically predicted angular distributions were used in our simulations. Legendre polyno-

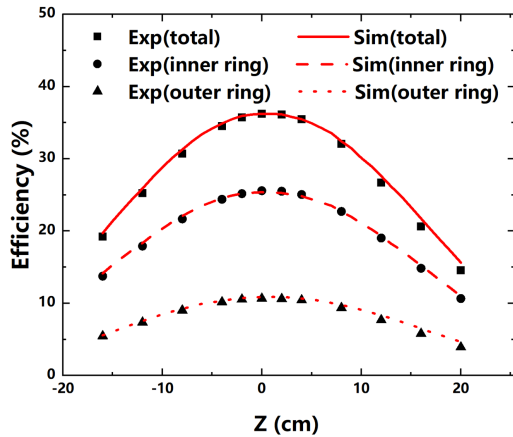


Fig. 6. (Color online) Detection efficiencies of the total (solid squares), the inner ring (solid circles) and the outer ring (solid triangles) detectors as a function of the target position. The statistical errors are smaller than the symbol size. Solid, dashed and long dashed curves are those from the Geant4 simulations.

mials up to the third order were used in calculating the angular distributions. Fig. 7 shows the Legendre polynomials coefficient a_1 used in the angular distributions of the $^{13}\text{C}(\alpha, n)^{16}\text{O}$ reaction as a function of beam energies in (a) and the representative angular distributions obtained at beam energies of 0.2, 0.7, 1.0534 and 1.2 MeV in (b). Adopting the angular distributions in Refs. [26–28], the angular distribution effect on the efficiencies is corrected in our Geant4 simulations.

Detection efficiencies were simulated using both isotropic and calculated angular distributions in the incident α energies between 0.2 - 3.15 MeV. In the simulation, the narrow resonances are ignored. Fig. 8 (a) shows simulated efficiencies using isotropic and calculated angular distributions. For α energies between 0.3 - 0.8 MeV, the difference is 0.19% - 2.28% which is relatively small. However, above 0.8 MeV, the difference becomes larger with a maximum of 4%. To evaluate the effect for the sharp resonance, we also simulated the detection efficiency at the energy where the a_1 coefficient reaches its maximum around $E = 1.0534$ MeV, as shown in Fig. 7 (a). The resulting efficiency is 11% less than the efficiency with an isotropic angular distribution. Therefore, the angular distribution effect needs to be evaluated carefully for the experiments aiming to a high precision.

The effects of the angular distributions were further investigated by comparing the simulated and measured ratios of the inner ring and outer ring detection efficiencies $R_{in/out}$. As shown in Fig. 8 (b), the $R_{in/out}$ is insensitive to the angular distribution and the simulations in both case agree reasonably well with the measured values from Ref. [30]. The difference between measured and simulated $R_{in/out}$ values is $\sim 4\%$. An alternative way of extrapolating the total detection efficiency was carried out as follows. The inner-ring detection efficiency is extrapolated to the neutron energy range relevant to the $^{13}\text{C}(\alpha, n)^{16}\text{O}$ reaction. Then the total detection efficiency is obtained using the measured $R_{in/out}$ values from Ref. [30]. The difference in the total detection efficiency

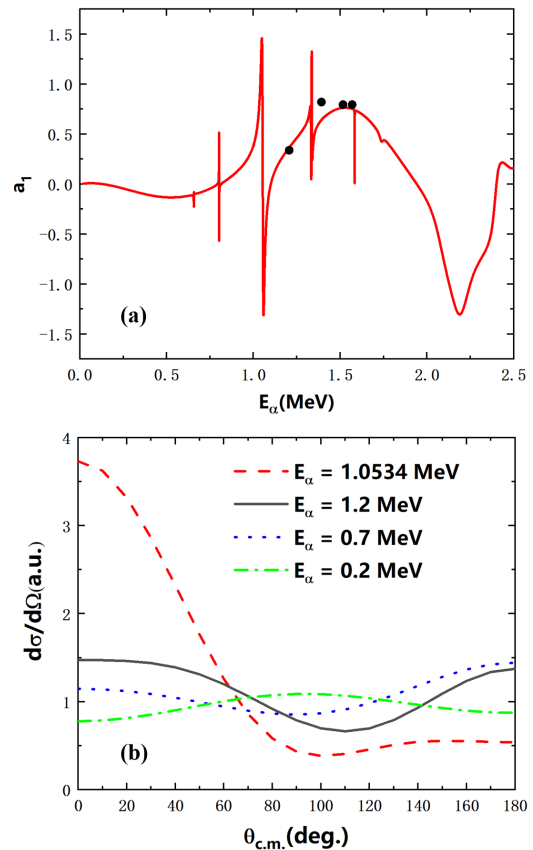


Fig. 7. (Color online) (a) Legendre polynomials coefficient a_1 used in the angular distributions of the $^{13}\text{C}(\alpha, n)^{16}\text{O}$ reaction as a function of beam energies. The red curve is from Paris/Hale ENDF-8 [26] and the black dots are from Ref [27]. In order to match the excitation energy of ^{17}O recommended by NNDC [29], the Legendre polynomials coefficients around 1.05 MeV and 1.33 MeV are shifted 2.4 keV and 1.7 keV, respectively, to higher energy. (b) Representative angular distributions obtained at beam energies of 0.2, 0.7, 1.0534 and 1.2 MeV.

between the two extrapolation methods is $\sim 2.5\%$, which is counted as another systematic uncertainty.

Taking into account the uncertainties of the Geant4 simulations (2.8%), the extrapolation (2.5%), the neutron angular distributions (2.3%) and the detection efficiency of HPGe detector (1.5%), the overall uncertainty of the detection efficiency for the $^{13}\text{C}(\alpha, n)^{16}\text{O}$ reaction in the energy range $E_\alpha = 300 - 800$ keV is determined to be 5%. Excluding the narrow resonances, the maximum uncertainty of neutron angular distributions is 4% if the energy range is extended up to 2.4 MeV. According to the ENDF angular distribution, the maximum uncertainty of neutron angular distributions at the energy beyond 2.4 MeV is 12%.

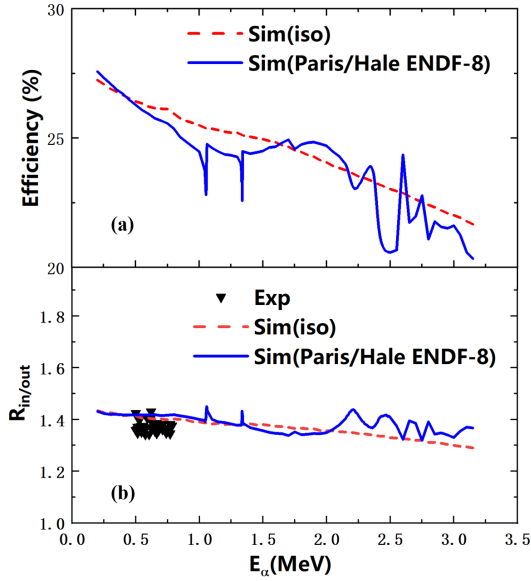


Fig. 8. (Color online) (a) Simulated detection efficiencies using isotropic (red dashed line) and theoretically predicted (blue solid line) angular distributions. (b) Simulated ratios $R_{in/out}$ using both isotropic (red dashed line) and theoretically predicted (blue solid line) angular distributions. Solid triangles are the measured $R_{in/out}$ from Ref. [30].

V. SUMMARY

A high-efficiency and low-background neutron detector array consisting of 24 ^3He proportional counters embed-

ded in a polyethylene moderator has been developed for the cross-section measurement of the $^{13}\text{C}(\alpha, n)^{16}\text{O}$ reaction at the China JinPing underground Laboratory. As a result of the deep underground location and a 5-cm thick borated polyethylene shield, a low background of 4.5(2)/hour was achieved, of which 1.94(5)/hour was from the internal α radioactivity. The $^{51}\text{V}(p, n)^{51}\text{Cr}$ reaction was used to calibrate the neutron detection efficiency of the array for neutrons with energies $E_n < 1$ MeV. For $E_n > 1$ MeV, the Monte Carlo simulation code Geant4 was used to extrapolate the detection efficiency. Specifically, an energy dependent detection efficiency, which can be directly applied to the $^{13}\text{C}(\alpha, n)^{16}\text{O}$ reaction, was obtained from the simulation. The effects of the angular distribution of the $^{13}\text{C}(\alpha, n)^{16}\text{O}$ reaction on the detection efficiency, which were overlooked in previous works, were investigated in the present work and shown to be non-negligible.

ACKNOWLEDGMENTS

The authors thank the staff of the 3MV tandetron accelerator facility of Sichuan University for their support during the experiment. The authors also thank the assistance of Carl Brune in estimating the corrections of the neutron angular distribution. This work was supported by the National Natural Science Foundation of China under Grants No. 11490564 and 11805138.

-
- [1] Roberto Gallino, Claudio Arlandini, Maurizio Busso, *et al.*, Evolution and Nucleosynthesis in Low-Mass Asymptotic Giant Branch Stars. II. Neutron Capture and the s-Process. *The Astrophysical Journal*, **497**, 388 (1998). DOI: [10.1086/305437](https://doi.org/10.1086/305437)
 - [2] B. Guo, Z. H. Li, M. Lugaro, *et al.*, NEW DETERMINATION OF THE $^{13}\text{C}(\alpha, n)^{16}\text{O}$ REACTION RATE AND ITS INFLUENCE ON THE s-PROCESS NUCLEOSYNTHESIS IN AGB STARS. *The Astrophysical Journal*, **756**: 193-195 (2012). DOI: [10.1088/0004-637x/756/2/193](https://doi.org/10.1088/0004-637x/756/2/193)
 - [3] deBoer, R. J., Brune, C. R., Febraro, M., *et al.*, Sensitivity of the $^{13}\text{C}(\alpha, n)^{16}\text{O}$ S factor to the uncertainty in the level parameters of the near-threshold state. *Phys. Rev. C*, **101**:045802 (2020). DOI: [10.1103/PhysRevC.101.045802](https://doi.org/10.1103/PhysRevC.101.045802)
 - [4] Falk Herwig, Marco Pignatari, Paul R. Woodward, *et al.*, CONVECTIVE-REACTIVE PROTON- ^{12}C COMBUSTION IN SAKURAI'S OBJECT (V4334 SAGITTARII) AND IMPLICATIONS FOR THE EVOLUTION AND YIELDS FROM THE FIRST GENERATIONS OF STARS. *The Astrophysical Journal*, **727** 89 (2011). DOI: [10.1088/0004-637x/727/2/89](https://doi.org/10.1088/0004-637x/727/2/89)
 - [5] Projjwal Banerjee, Yong-Zhong Qian, Alexander Heger, New Neutron-capture Site in Massive Pop III and Pop II Stars as a Source for Heavy Elements in the Early Galaxy. *The Astrophysical Journal*, **865** 120 (2018). DOI: [10.3847/1538-4357/aadb8c](https://doi.org/10.3847/1538-4357/aadb8c)
 - [6] Drotleff, H. W., Denker, A., Knee, H., *et al.*, Reaction Rates of the s-Process Neutron Sources $^{22}\text{Ne}(\alpha, n)^{25}\text{Mg}$ and $^{13}\text{C}(\alpha, n)^{16}\text{O}$. *The Astrophysical Journal*, **414** 735 (1993). DOI: [10.1086/173119](https://doi.org/10.1086/173119)
 - [7] Harissopoulos, S., Becker, H. W., Hammer, J. W., *et al.*, Cross section of the $^{13}\text{C}(\alpha, n)^{16}\text{O}$ reaction: A background for the measurement of geo-neutrinos. *Phys. Rev. C*, **72** 062801 (2005). DOI: [10.1103/PhysRevC.72.062801](https://doi.org/10.1103/PhysRevC.72.062801)
 - [8] Cheng, Jian-Ping, Kang, Ke-Jun, Li, Jian-Min, *et al.*, The China Jinping Underground Laboratory and Its Early Science. *PAnnual Review of Nuclear and Particle Science*, **67** 231-251 (2017). DOI: [10.1146/annurev-nucl-102115-044842](https://doi.org/10.1146/annurev-nucl-102115-044842)
 - [9] Li, Zi-Yuan, Zhang, Yu-Mei, Cao, Guo-Fu, *et al.*, Event vertex and time reconstruction in large-volume liquid scintillator detectors. *NUCL SCI TECH*, **32** 49 (2021). DOI: [10.1007/s41365-021-00885-z](https://doi.org/10.1007/s41365-021-00885-z)
 - [10] Giboni, Karl Ludwig, Juyal, Pratibha, Aprile, Elena, *et al.*, A LN_2 -based cooling system for a next-generation liquid xenon dark matter detector. *NUCL SCI TECH*, **31** 76 (2020). DOI: [10.1007/s41365-020-00786-7](https://doi.org/10.1007/s41365-020-00786-7)
 - [11] Juyal, Pratibha, Giboni, Karl Ludwig, Ji, Xiang-Dong, *et al.*, On proportional scintillation in very large liquid xenon detectors. *NUCL SCI TECH*, **31** 93 (2020). DOI: [10.1007/s41365-020-00797-4](https://doi.org/10.1007/s41365-020-00797-4)

- [12] Liu, WeiPing, Li, ZhiHong, He, JiangJun, Tang, XiaoDong, *et al.*, Progress of Jinping Underground laboratory for Nuclear Astrophysics (JUNA). *Science China Physics, Mechanics & Astronomy*, **59** 4 (2016). DOI: [10.1007/s11433-016-5785-9](https://doi.org/10.1007/s11433-016-5785-9)
- [13] Zhang, L. Y., Su, J., He, J. J., *et al.*, Direct Measurement of the Astrophysical $^{19}\text{F}(p, \alpha\gamma)^{16}\text{O}$ Reaction in the Deepest Operational Underground Laboratory. *Phys. Rev. Lett.*, **127** 152702 (2021). DOI: [10.1103/PhysRevLett.127.152702](https://doi.org/10.1103/PhysRevLett.127.152702)
- [14] Sascha Falahat, Andreas Best, Manoel Couder, *et al.*, A 3He neutron detector for the measurement of (α, n) reactions. *Nuclear Instruments and Methods in Physics Research Section A: Accelerators, Spectrometers, Detectors and Associated Equipment*, **700** 53-58 (2013). DOI: [10.1016/j.nima.2012.10.036](https://doi.org/10.1016/j.nima.2012.10.036)
- [15] T.J. Langford, C.D. Bass, E.J. Beise, *et al.*, Event identification in 3He proportional counters using rise-time discrimination. *Nuclear Instruments and Methods in Physics Research Section A: Accelerators, Spectrometers, Detectors and Associated Equipment*, **717** 51-57 (2013). DOI: [10.1016/j.nima.2013.03.062](https://doi.org/10.1016/j.nima.2013.03.062)
- [16] L. Csedreki, G.F. Ciani, J. Balibrea-Correa, *et al.*, Characterization of the LUNA neutron detector array for the measurement of the $^{13}\text{C}(\alpha, n)^{16}\text{O}$ reaction. *Nuclear Instruments and Methods in Physics Research Section A: Accelerators, Spectrometers, Detectors and Associated Equipment*, **994** 165081 (2021). DOI: [10.1016/j.nima.2021.165081](https://doi.org/10.1016/j.nima.2021.165081)
- [17] H.X. Huang, B. Gao, Y.T. Li, *et al.*, Low event rate neutron detector array using the coincidence between plastic scintillator and Helium-3 proportional counters. *Nuclear Instruments and Methods in Physics Research Section A: Accelerators, Spectrometers, Detectors and Associated Equipment*, **1003** 165323 (2021). DOI: [10.1016/j.nima.2021.165323](https://doi.org/10.1016/j.nima.2021.165323)
- [18] Jifeng Han, Zhu An, Gaoqun Zheng, *et al.*, An ion beam facility based on a 3 MV tandetron accelerator in Sichuan University, China. *Nuclear Instruments and Methods in Physics Research Section B: Beam Interactions with Materials and Atoms*, **418** 68-73 (2021). DOI: [10.1016/j.nimb.2018.01.002](https://doi.org/10.1016/j.nimb.2018.01.002)
- [19] Deconninck, G. and Royen, J., La reaction $^{51}\text{V}(p, n)^{51}\text{Cr}$ comme source de neutrons monoenergetiques. *Nuclear Instruments and Methods*, **75** 266-270(1969). DOI: [10.1016/0029-554X\(69\)90607-7](https://doi.org/10.1016/0029-554X(69)90607-7)
- [20] J. Pereira, P. Hosmer, G. Lorusso, *et al.*, The neutron long counter NERO for studies of β -delayed neutron emission in the r-process. *Nuclear Instruments and Methods in Physics Research Section A: Accelerators, Spectrometers, Detectors and Associated Equipment*, **618** 275-283(2010). DOI: [10.1016/j.nima.2010.02.262](https://doi.org/10.1016/j.nima.2010.02.262)
- [21] E. Ramström, T. Wiedling, The excitation function of the $^{13}\text{C}(\alpha, n)^{16}\text{O}$ reaction and its astrophysical application. *Nuclear Physics A*, **272** 259-268(1976). DOI: [10.1016/0375-9474\(76\)90330-4](https://doi.org/10.1016/0375-9474(76)90330-4)
- [22] Lund, Eva, Hoff, P., Aleklett, Kjell, *et al.*, Delayed neutron emission probabilities of gallium, bromine, rubidium, indium, antimony, iodine, and cesium precursors. *Zeitschrift für Physik A Atoms and Nuclei*, **294** (1980). DOI: [10.1007/BF01438160](https://doi.org/10.1007/BF01438160)
- [23] S. Agostinelli, J. Allison, K. Amako, *et al.*, Geant4—a simulation toolkit. *Nuclear Instruments and Methods in Physics Research Section A: Accelerators, Spectrometers, Detectors and Associated Equipment*, **506** 250-303(2003). DOI: [10.1016/S0168-9002\(03\)01368-8](https://doi.org/10.1016/S0168-9002(03)01368-8)
- [24] J. Allison, K. Amako, J. Apostolakis *et al.*, Recent developments in Geant4. *Nuclear Instruments and Methods in Physics Research Section A: Accelerators, Spectrometers, Detectors and Associated Equipment*, **835** 186-225(2016). DOI: [10.1016/j.nima.2016.06.125](https://doi.org/10.1016/j.nima.2016.06.125)
- [25] A.J. Koning and D. Rochman, Modern Nuclear Data Evaluation with the TALYS Code System. *Nuclear Data Sheets*, **113** 2841-2934(2012). DOI: [10.1016/j.nds.2012.11.002](https://doi.org/10.1016/j.nds.2012.11.002)
- [26] D.A. Brown, M.B. Chadwick, R. Capote *et al.*, ENDF/B-VIII.0: The 8th Major Release of the Nuclear Reaction Data Library with CIELO-project Cross Sections, New Standards and Thermal Scattering Data. *Nuclear Data Sheets*, **148** 1-142(2018). DOI: [10.1016/j.nds.2018.02.001](https://doi.org/10.1016/j.nds.2018.02.001)
- [27] Walton, R. B., Clement, J. D., Boreli, F., Interaction of Neutrons with Oxygen and a Study of the $\text{C}^{13}(\alpha, n)\text{O}^{16}$ Reaction. *Phys. Rev.*, **107** 1065-1075(1957). DOI: [10.1103/PhysRev.107.1065](https://doi.org/10.1103/PhysRev.107.1065)
- [28] C.Brune, Personal conversation. *Phys. Rev.*, (2021)
- [29] National Nuclear Data Center. <https://www.nndc.bnl.gov/nudat3/getdatasetClassic.jsp?nucle-us=170&unc>
- [30] B. Gao., *et al.*, Submitted to *Phys. Rev. Lett.*. (2021)